RAYLEIGH–TAYLOR INSTABILITIES WITH SHEARED MAGNETIC FIELDS

M. S. RUDERMAN[1,2], J. TERRADAS[3], AND J. L. BALLESTER[3]
[1] Solar Physics and Space Plasma Research Centre (SP²RC), University of Sheffield, Hicks Building, Hounsfield Road, Sheffield S3 7RH, UK
[2] Space Research Institute (IKI) Russian Academy of Sciences, Moscow, Russia
[3] Departament de Física, Universitat de les Illes Balears, E-07122 Palma de Mallorca, Spain

ABSTRACT

Magnetic Rayleigh–Taylor (MRT) instabilities may play a relevant role in many astrophysical problems. In this work the effect of magnetic shear on the growth rate of the MRT instability is investigated. The eigenmodes of an interface and a slab model under the presence of gravity are analytically calculated assuming that the orientation of the magnetic field changes in the equilibrium, i.e., there is magnetic shear. We solve the linearized magnetohydrodynamic equations in the incompressible regime. We find that the growth rate is bounded under the presence of magnetic shear. We have derived simple analytical expressions for the maximum growth rate, corresponding to the most unstable mode of the system. These expressions provide the explicit dependence of the growth rate on the various equilibrium parameters. For small angles the growth time is linearly proportional to the shear angle, and in this regime the single interface problem and the slab problem tend to the same result. On the contrary, in the limit of large angles and for the interface problem the growth time is essentially independent of the shear angle. In this regime we have also been able to calculate an approximate expression for the growth time for the slab configuration. Magnetic shear can have a strong effect on the growth rates of the instability. As an application of the results found in this paper we have indirectly determined the shear angle in solar prominence threads using their lifetimes and the estimation of the Alfvén speed of the structure.

Key words: magnetohydrodynamics (MHD) – plasmas – Sun: corona – Sun: oscillations – waves

Online-only material: color figures

1. INTRODUCTION

The magnetic Rayleigh–Taylor (MRT) instability is important in many astrophysical systems. Some examples are buoyant magnetized bubbles identified in clusters of galaxies (see Robinson et al. (2004) and Jones & De Young (2005) for studies in two-dimensional (2D), and O'Neill et al. (2009) for three-dimensional (3D) configurations). MRT instabilities also manifest themselves in shells of young supernova remnants, this has been investigated by Jun et al. (1995) in 2D and 3D Cartesian configurations and by Jun & Norman (1996) in 3D using spherical coordinates. Bucciantini et al. (2004) have numerically investigated the development of the MRT instability at the interface between an expanding pulsar wind nebula and its surrounding supernova remnant. Stone & Gardiner (2007) studied the behavior of MRT instability in three dimensions with special focus on the structure and dynamics of the nonlinear evolution of the system. They analyzed various configurations including the situation in which magnetic fields change direction at the interface between the two fluids. Stone & Gardiner (2007) used the MRT instability to explain the structure of the optical filaments observed in the Crab nebula.

In laboratory plasmas the possible stabilizing effect by a force-free magnetic field has been studied in the past by many authors (see for example Goedbloed 1971a, 1971b, 1971c; Goedbloed & Poedts 2004) using the single interface problem and the slab problem and applying vacuum conditions at some of the boundaries. Yang et al. (2011) have studied the magnetic field transition layer effects on the MRT instability with continuous magnetic field and density profiles and have found that the linear growth rate of the MRT instability increases with the thickness of the magnetic field transition layer, especially for the case of small thickness. Recently, Zhang et al. (2012) have used the

ideal magnetohydrodynamic (MHD) model to study the effect of magnetic shear in a finite slab representing a magnetic liner, which is a device used in experiments with fusion plasmas. These authors have found that magnetic shear reduces the MRT growth rate in general.

The emergence of magnetic flux from the solar interior and the formation of flux tubes is another example where MRT instabilities are relevant. For example, Isobe et al. (2005, 2006) proposed that the MRT instability is a possible cause of the filamentary structure in mass and current density in the emerging flux regions. In the solar atmosphere, Ryutova et al. (2010) suggested that several dynamic processes taking place in prominences are most probably related to MRT instabilities. Along this line of work, Hillier et al. (2011, 2012a, 2012b) have performed 3D MHD simulations to investigate the nonlinear evolution of the Kippenhahn–Schlüter prominence model to the MRT instability.

The fine structure of solar prominences reveals the presence of magnetic threads. These structures are quite thin, of the order of 100 km, aligned with the magnetic field and, in many cases, they seem to lie horizontally with respect to the photosphere (see DeVore 2012, 2013, for recent results about the formation of these structures). Terradas et al. (2012) have considered the possible link between MRT instabilities and the short thread lifetimes. In that work a slab model permeated by a horizontal magnetic field was considered. The growth rates of the unstable modes and the thresholds for stability were determined analytically. In the present paper we extend the study to the situation with a sheared magnetic field in which the magnetic field changes its direction at the interfaces of the plasma slab. To understand the results in the slab model we describe first the effect of shear at a single plasma interface. Magnetic shear introduces changes in the growth rates of the
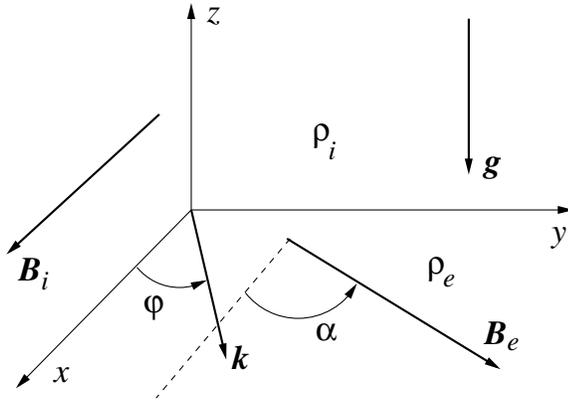
Figure 1. Sketch of a single magnetic interface.

unstable modes that might be relevant regarding the lifetime of threads. In this work we analytically calculate these growth rates and perform a detailed analysis of their dependence on the equilibrium parameters.

2. PROBLEM FORMULATION

To describe the plasma motion we use the linearized ideal MHD equations for incompressible plasmas

$$\nabla \cdot \boldsymbol{\xi} = 0, \tag{1}$$

$$\rho \frac{\partial^2 \boldsymbol{\xi}}{\partial t^2} = -\nabla p + \frac{1}{\mu_0}(\nabla \times \boldsymbol{b}) \times \boldsymbol{B}, \tag{2}$$

$$\boldsymbol{b} = \nabla \times (\boldsymbol{\xi} \times \boldsymbol{B}). \tag{3}$$

Here $\boldsymbol{\xi}$ is the plasma displacement related to the plasma velocity $\boldsymbol{u}$ by $\boldsymbol{u} = \partial \boldsymbol{\xi}/\partial t$, p the pressure perturbation, and $\boldsymbol{b}$ the magnetic field perturbation; $\boldsymbol{B}$ is the background magnetic field, ρ the plasma density assumed to be piecewise constant, and μ_0 the magnetic permeability of free space. When deriving Equations (1)–(3) we have assumed that the equilibrium is static and current-free, e.g., $\nabla \times \boldsymbol{B} = 0$.

In what follows we consider two equilibrium states. In the first one there are two semi-infinite regions separated by the xy-plane in Cartesian coordinates x, y, z with the z-axis in the vertical direction (see Figure 1). The plasma density and background magnetic field are constant in the two regions, and they are given by

$$\rho = \begin{cases} \rho_e, & z < 0, \\ \rho_i, & z > 0, \end{cases} \quad \boldsymbol{B} = \begin{cases} \boldsymbol{B}_e, & z < 0, \\ \boldsymbol{B}_i, & z > 0. \end{cases} \tag{4}$$

The background magnetic field is assumed to be parallel to the xy-plane. The equilibrium pressure P is defined by the equation

$$\frac{dP}{dz} = -g\rho, \tag{5}$$

where g is the gravity acceleration. The total pressure, magnetic plus kinetic, has to be continuous at $z = 0$. The solution to Equation (5) satisfying this condition is

$$P = \begin{cases} P_0 - \dfrac{B_e^2}{2\mu_0} - g\rho_e z, & z < 0, \\[2ex] P_0 - \dfrac{B_i^2}{2\mu_0} - g\rho_i z, & z > 0, \end{cases} \tag{6}$$
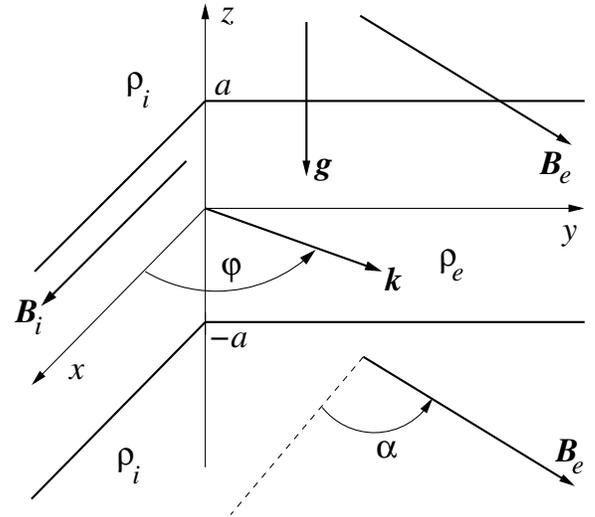
where P_0 is an arbitrary constant. We call this equilibrium state the single magnetic interface.

In the second equilibrium state there are three regions separated by horizontal planes at $z = \pm a$ (see Figure 2). The plasma density and background magnetic field are the same in two semi-infinite regions, and they are given by

$$\rho = \begin{cases} \rho_e, & z < -a, \\ \rho_i, & |z| < a, \\ \rho_e, & z > a, \end{cases} \quad \boldsymbol{B} = \begin{cases} \boldsymbol{B}_e, & z < -a, \\ \boldsymbol{B}_i, & |z| < a, \\ \boldsymbol{B}_e, & z > a. \end{cases} \tag{7}$$

The background magnetic field is once again assumed to be parallel to the xy-plane. The total pressure has to be continuous at $z = \pm a$. The solution to Equation (5) satisfying this condition is

$$P = \begin{cases} P_0 - \dfrac{B_e^2}{2\mu_0} + ga(\rho_i - \rho_e) - g\rho_e z, & z < -a, \\[2ex] P_0 - \dfrac{B_i^2}{2\mu_0} - g\rho_i z, & |z| < a, \\[2ex] P_0 - \dfrac{B_e^2}{2\mu_0} - ga(\rho_i - \rho_e) - g\rho_e z, & z > a. \end{cases} \tag{8}$$

This second configuration is called the magnetic slab.

At the boundaries separating regions with different plasma densities and background magnetic field the plasma displacement in the z-direction and the Lagrangian perturbation of the total pressure have to be continuous. Hence, we have two boundary conditions,

$$[\xi_z] = 0, \quad [p_T - g\rho\xi_z] = 0, \tag{9}$$

where the square brackets denote the jump of a quantity across a discontinuity, and $p_T = p + \boldsymbol{B} \cdot \boldsymbol{b}/\mu_0$ is the perturbation of the total pressure. When deriving the second boundary condition we have used Equation (5). The boundary conditions (9) have to be satisfied at $z = 0$ in the case of the single magnetic interface, and at $z = \pm a$ in the case of the magnetic slab. One additional boundary condition is that all perturbations have to vanish as $|z| \to \infty$.

Equations (1)–(3) together with the boundary conditions (9) are used in the next section to derive the dispersion relations determining the stability of the two equilibrium configurations.

Figure 2. Sketch of the magnetic slab.

3. DERIVATION OF THE DISPERSION RELATIONS

We Fourier-analyze the perturbations of all quantities and take them proportional to $\exp[i(\mathbf{k} \cdot \mathbf{r} - \omega t)]$, where $\mathbf{k} = (k_x, k_y, 0)$ and $\mathbf{r} = (x, y, z)$. Then Equations (1)–(3) reduce to

$$\frac{d\xi_z}{dz} + i\mathbf{k} \cdot \boldsymbol{\xi} = 0, \tag{10}$$

$$\rho\omega^2 \boldsymbol{\xi}_\perp = i\mathbf{k}\, p_T - \frac{i}{\mu_0} \mathbf{b}_\perp (\mathbf{k} \cdot \mathbf{B}), \tag{11}$$

$$\rho\omega^2 \xi_z = \frac{dp_T}{dz} - \frac{i}{\mu_0} b_z (\mathbf{k} \cdot \mathbf{B}), \tag{12}$$

$$\mathbf{b} = i(\mathbf{k} \cdot \mathbf{B})\boldsymbol{\xi}, \tag{13}$$

where $\boldsymbol{\xi}_\perp$ and $\mathbf{b}_\perp$ are the components of the plasma displacement and magnetic field perturbation orthogonal to the z-axis. Eliminating all the variables from Equations (10)–(13) in favor of ξ_z we obtain the equation for this variable,

$$\frac{d^2\xi_z}{dz^2} - k^2 \xi_z = 0. \tag{14}$$

In addition, we obtain the expression of p_T in terms of ξ_z,

$$p_T = \frac{\rho(\omega^2 - \omega_A^2)}{k^2} \frac{d\xi_z}{dz}, \tag{15}$$

where ω_A is the Alfvén frequency defined by

$$\omega_A^2 = \frac{(\mathbf{k} \cdot \mathbf{B})^2}{\mu_0 \rho}. \tag{16}$$

This expression enables us to rewrite the boundary conditions (9) in terms of ξ_z as

$$[\xi_z] = 0, \quad \left[\rho(\omega^2 - \omega_A^2)\frac{d\xi_z}{dz} - g\rho k^2 \xi_z\right] = 0. \tag{17}$$

3.1. Dispersion Relation for a Single Magnetic Interface

In the case of a single magnetic interface the solution to Equation (14), satisfying the first boundary condition in Equation (17) at $z = 0$ and decaying as $|z| \to \infty$, is given, with the accuracy up to an arbitrary multiplicative constant, by

$$\xi_z = \begin{cases} e^{kz}, & z < 0, \\ e^{-kz}, & z > 0. \end{cases} \tag{18}$$

Substituting this solution in the second boundary condition in Equation (17) we obtain the following dispersion relation

$$\omega^2 = \frac{\rho_e \omega_{Ae}^2 + \rho_i \omega_{Ai}^2 + gk(\rho_e - \rho_i)}{\rho_e + \rho_i}. \tag{19}$$

This is the well-known dispersion equation for the interface problem in an incompressible fluid (Chandrasekhar 1961). When $g = 0$ this is the dispersion equation for surface waves on a magnetic interface (e.g., Roberts 1981). On the other hand, when there is no magnetic field, this dispersion equation determines the Rayleigh–Taylor instability of the interface between two incompressible fluids (Rayleigh 1883; Taylor 1950).

3.2. Dispersion Relation for the Magnetic Slab

Now we proceed to the derivation of the dispersion equation for the magnetic slab. The general solution to Equation (14) continuous at $z = \pm a$ and decaying as $|z| \to \infty$ is

$$\xi_z = \begin{cases} [C_1 \cosh(ka) - C_2 \sinh(ka)]\, e^{k(z+a)}, & z < -a, \\ C_1 \cosh(kz) + C_2 \sinh(kz), & |z| < a, \\ [C_1 \cosh(ka) + C_2 \sinh(ka)]\, e^{-k(z-a)}, & z > a, \end{cases} \tag{20}$$

where C_1 and C_2 are arbitrary constants. Substituting this solution in the second boundary condition in Equation (17) we obtain two equations,

$$A_{11}C_1 - A_{12}C_2 = 0, \quad A_{21}C_1 + A_{22}C_2 = 0, \tag{21}$$

where

$$\begin{aligned}
A_{11} &= \rho_e(\omega^2 - \omega_{Ae}^2) + gk(\rho_i - \rho_e) + \rho_i(\omega^2 - \omega_{Ai}^2)\tanh(ka), \\
A_{12} &= [\rho_e(\omega^2 - \omega_{Ae}^2) + gk(\rho_i - \rho_e)]\tanh(ka) + \rho_i(\omega^2 - \omega_{Ai}^2), \\
A_{21} &= \rho_e(\omega^2 - \omega_{Ae}^2) - gk(\rho_i - \rho_e) + \rho_i(\omega^2 - \omega_{Ai}^2)\tanh(ka), \\
A_{22} &= [\rho_e(\omega^2 - \omega_{Ae}^2) - gk(\rho_i - \rho_e)]\tanh(ka) + \rho_i(\omega^2 - \omega_{Ai}^2).
\end{aligned} \tag{22}$$

The system (21) of linear homogeneous equations for C_1 and C_2 has non-trivial solutions when its determinant is zero. This condition is written as $A_{11}A_{22} + A_{12}A_{21} = 0$. After some algebra this equation gives

$$\begin{aligned}
&\omega^4[2\rho_e\rho_i + (\rho_e^2 + \rho_i^2)\tanh(2ka)] - 2\omega^2[\rho_e\rho_i(\omega_{Ae}^2 + \omega_{Ai}^2) \\
&\quad + (\rho_e^2\omega_{Ae}^2 + \rho_i^2\omega_{Ai}^2)\tanh(2ak)] + 2\rho_e\rho_i\omega_{Ae}^2\omega_{Ai}^2 \\
&\quad + (\rho_e^2\omega_{Ae}^4 + \rho_i^2\omega_{Ai}^4)\tanh(2ak) \\
&\quad - g^2k^2(\rho_e - \rho_i)^2\tanh(2ak) = 0.
\end{aligned} \tag{23}$$

The two solutions to this dispersion equation are ω_+^2 and ω_-^2 given by

$$\omega_\pm^2 = \frac{F \pm G}{H}, \tag{24}$$

where

$$F = \rho_i\rho_e(\omega_{Ai}^2 + \omega_{Ae}^2)\cosh(2ka) + (\rho_i^2\omega_{Ai}^2 + \rho_e^2\omega_{Ae}^2)\sinh(2ka), \tag{25}$$

$$\begin{aligned}
G = \big\{&\rho_i^2\rho_e^2(\omega_{Ai}^2 - \omega_{Ae}^2)^2 + g^2k^2(\rho_i - \rho_e)^2 \\
&\times [(\rho_i^2 + \rho_e^2)\sinh^2(2ka) + \rho_i\rho_e\sinh(4ka)]\big\}^{1/2},
\end{aligned} \tag{26}$$

$$H = 2\rho_i\rho_e\cosh(2ka) + (\rho_i^2 + \rho_e^2)\sinh(2ka). \tag{27}$$

When $g = 0$ the dispersion relation given by Equation (24) describes waves in a magnetic slab (e.g., Parker 1974; Edwin & Roberts 1982). The plus sign corresponds to kink waves where $\xi_z(z)$ is an even function of z, while the minus sign corresponds to sausage waves where $\xi_z(z)$ is an odd function of z. Although, when $g \neq 0$, $\xi_z(z)$ is neither odd nor even in both perturbation modes described by Equation (24), we will still use the name "kink" for modes with the plus sign, and "sausage" for modes with the minus sign. It can be also shown that Equation (24) in the absence of magnetic shear reduces to Equation (22) in Terradas et al. (2012).

4. INVESTIGATION OF STABILITY

Here we use the dispersion equations derived in the previous section to study the stability of a single magnetic interface and a magnetic slab.

4.1. Stability of a Single Magnetic Interface

Without loss of generality we can choose the x-axis in the direction of the vector $\boldsymbol{B}_i$. It is convenient to introduce the angle φ between the x-axis and the wave vector $\boldsymbol{k}$. Then we write $\boldsymbol{k} = k(\cos\varphi, \sin\varphi, 0)$, and we also introduce the angle α between $\boldsymbol{B}_e$ and $\boldsymbol{B}_i$, so $\boldsymbol{B}_e = B_e(\cos\alpha, \sin\alpha, 0)$. Since the MHD equations are invariant under the substitution $-\boldsymbol{B}$ for $\boldsymbol{B}$, we can always choose such the direction of vector $\boldsymbol{B}_e$ that the angle α is either acute or right. Hence, in what follows we assume that $0 \leqslant \alpha \leqslant \pi/2$. Finally, we introduce the dimensionless parameters $\zeta = \rho_i/\rho_e$ and $\chi = B_i/B_e$. We rewrite Equation (19) as

$$\omega^2 = \frac{g^2 h}{V_{Ae}^2} \frac{h[\chi^2 \cos^2\varphi + \cos^2(\varphi - \alpha)] + 1 - \zeta}{\zeta + 1}, \quad (28)$$

where the Alfvén speed in the lower medium, V_{Ae}, and the dimensionless wave number h are defined by

$$V_{Ae}^2 = \frac{B_e^2}{\mu_0 \rho_e}, \quad h = \frac{V_{Ae}^2 k}{g}. \quad (29)$$

A well-known result is that the interface is stable when $\zeta < 1$, i.e., when the density of the upper medium is smaller than that of the lower medium. In the opposite situation, i.e., when $\zeta > 1$, there is a qualitative difference between the case where the magnetic field is in the same direction at the two sides of the interface ($\alpha = 0$), and the case where the magnetic field is sheared ($\alpha \neq 0$). In the first case perturbations with the wave vector perpendicular to the magnetic field ($\varphi = \pi/2$) are unstable for any value of the dimensionless wave number h. Since, for such perturbations, the instability increment or growth rate is equal to

$$\sqrt{gk\frac{\zeta - 1}{\zeta + 1}},$$

the instability growth rate is unbounded. This means that the initial value problem describing the evolution of the interface initial perturbation is ill-posed. Of course, the growth rate will be bounded and the problem will be well-posed if we take into account either dissipation or the finite thickness of the transition between the two homogeneous regions.

In the second case ($\alpha \neq 0$) perturbations with a fixed direction of the wave number defined by the angle φ are unstable only when

$$h < h_c(\varphi) = \frac{\zeta - 1}{\chi^2 \cos^2\varphi + \cos^2(\varphi - \alpha)}. \quad (30)$$

In Figure 3 we have plotted the square of ω as a function of h and φ. The continuous curve corresponds to $\omega = 0$ and separates the regions between stable and unstable modes. In fact all perturbations with the wave number larger than $\bar{h}_c$ are stable, where

$$\bar{h}_c = \max_\varphi h_c(\varphi) = h_c(\varphi_c)$$

$$= \frac{\zeta - 1}{2\chi^2 \sin^2\alpha}(\chi^2 + 1 + \sqrt{\chi^4 + 2\chi^2 \cos 2\alpha + 1}), \quad (31)$$
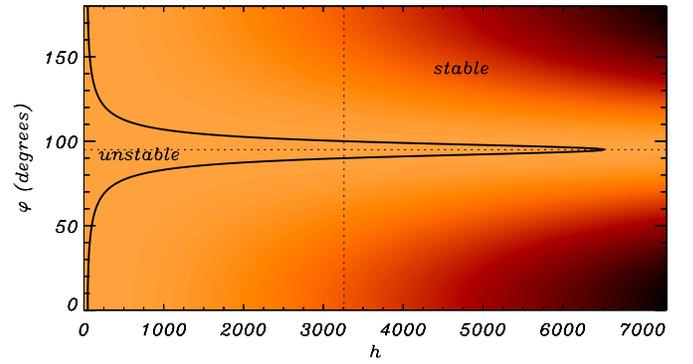
Figure 3. Square of the frequency (in arbitrary units) as a function of the dimensionless number h and φ for the interface. The continuous curve corresponds to $\omega = 0$ and represents the transition between stable and unstable modes. The horizontal and vertical dotted lines, respectively, represent the critical angle φ_c, and the wave number $\bar{h}_c/2$ at which the increment takes its maximum value. In this plot, $\alpha = 10°$, $\chi = 1$, and $\zeta = 100$.
(A color version of this figure is available in the online journal.)

and

$$\varphi_c = \frac{1}{2} \arctan\frac{\sin 2\alpha}{\chi^2 + \cos 2\alpha} + \frac{\pi}{2}. \quad (32)$$

Note that φ_c is defined with the accuracy up to an additive constant multiple to π.

It turns out that the instability increment takes its maximum value γ_m for a harmonic perturbation with the dimensionless wave number $\bar{h}_c/2$ (see vertical line in Figure 3) and propagating at either the angle φ_c (see horizontal line in Figure 3) or $\varphi_c + \pi$. This maximum value is given by

$$\gamma_m = \frac{g}{2V_{Ae}}\sqrt{\bar{h}_c \frac{\zeta - 1}{\zeta + 1}}. \quad (33)$$

Hence, in the case of sheared magnetic field, the perturbation growth rate is bounded, and the initial value problem is well-posed.

The external and internal Alfvén speed satisfy the following relationship

$$V_{Ae} = V_{Ai}\frac{\sqrt{\zeta}}{\chi}, \quad (34)$$

and now we rewrite Equation (33) in terms of the internal Alfvén speed,

$$\gamma_m = \frac{g|\zeta - 1|}{2\sqrt{2}V_{Ai}\sin\alpha}\sqrt{\frac{\chi^2 + 1 + \sqrt{\chi^4 + 2\chi^2 \cos 2\alpha + 1}}{\zeta(\zeta + 1)}}. \quad (35)$$

It is interesting to study the dependence of the growth time, defined as $\tau_g = 1/\gamma_m$, on the equilibrium parameters. In Figure 4 the 2D dependence of τ_g is represented as a function of α and χ for $\zeta = 100$. We do see that a given growth time can be obtained by the proper combination of the parameters α, χ, and V_{Ai}. Note that, for small angles, a larger Alfvén speed is required to obtain the same growth rate. In fact, Equation (35) is further simplified if we take the limit of small shear angles ($\alpha \ll 1$),

$$\gamma_m \approx \frac{g|\zeta - 1|}{2\alpha V_{Ai}}\sqrt{\frac{\chi^2 + 1}{\zeta(\zeta + 1)}}. \quad (36)$$

This expression explains why decreasing α while keeping γ_m constant requires an increase of the internal Alfvén speed (if
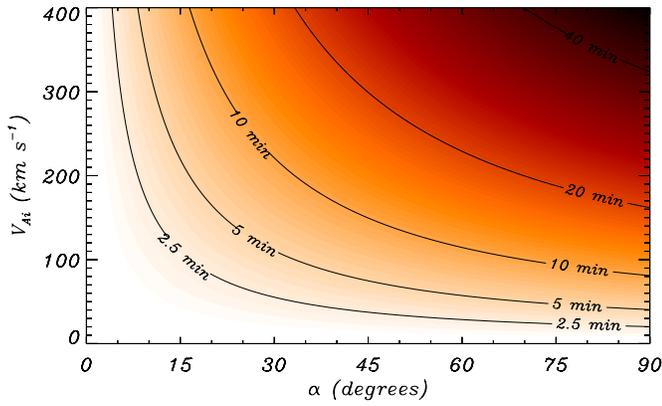
Figure 4. Growth time $\tau_g = 1/\gamma_m$ of the MRT most unstable mode at a single interface as a function of the shear angle α and V_{Ai} for $\chi = 1$ and $\zeta = 100$. (A color version of this figure is available in the online journal.)

the rest of the parameters, i.e., g, χ, and ζ are constant). In the opposite limit, i.e., when $\alpha \approx \pi/2$, Equation (35) reduces to

$$\gamma_m \approx \frac{g}{2V_{Ai}} \frac{|\zeta - 1|}{\sqrt{\zeta(\zeta + 1)}} \Theta. \tag{37}$$

where

$$\Theta = \begin{cases} \chi, & \chi > 1, \\ 1, & \chi \leqslant 1. \end{cases} \tag{38}$$

Thus, as Figure 4 indicates, for configurations with a strong shear the curve of the growth time is almost horizontal since, according to Equation (37), it is independent of α. Note that for $\chi < 1$ the growth time is independent of χ while it is linearly proportional to χ for $\chi > 1$. Finally note that the factor that contains the dependence with ζ in the previous expressions is approximately 1 in the limit of $\zeta \gg 1$. Then Equations (35)–(37) can be further simplified for configurations with a high density contrast.

4.2. Stability of a Magnetic Slab

Since now there is a natural spatial scale a, it is convenient to introduce a new dimensionless wave number $\kappa = ak$. We also introduce the parameter characterizing the relative strength of magnetic field and gravity, $\sigma = V_{Ae}^2/(ag)$. Otherwise we use the same dimensionless parameters as in the previous section. Then we rewrite Equation (24) as

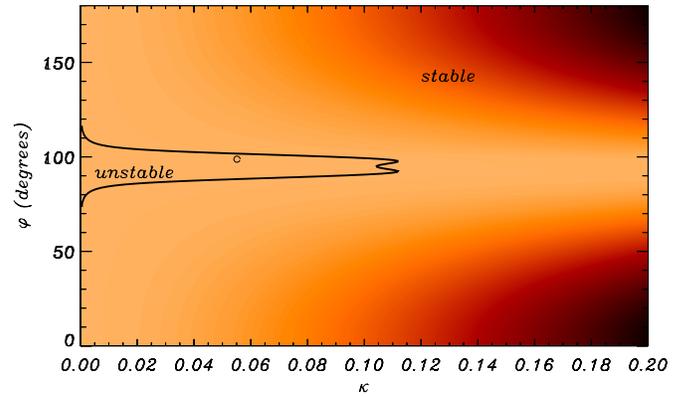$$\omega_{\pm}^2 = \frac{g(\tilde{F} \pm \tilde{G})}{a\tilde{H}}, \tag{39}$$

where

$$\tilde{F} = \sigma \kappa^2 \{[\chi^2 \cos^2 \varphi + \zeta \cos^2(\varphi - \alpha)] \cosh 2\kappa \\ + [\zeta \chi^2 \cos^2 \varphi + \cos^2(\varphi - \alpha)] \sinh 2\kappa\}, \tag{40}$$

$$\tilde{G} = \{\sigma^2 \kappa^4 [\chi^2 \cos^2 \varphi - \zeta \cos^2(\varphi - \alpha)]^2 \\ + \kappa^2(\zeta - 1)^2 [(\zeta^2 + 1) \sinh^2 2\kappa + \zeta \sinh 4\kappa]\}^{1/2}, \tag{41}$$

$$\tilde{H} = 2\zeta \cosh 2\kappa + (\zeta^2 + 1) \sinh 2\kappa. \tag{42}$$

It is obvious that only ω_-^2 can be negative, while ω_+^2 is always positive. Hence, only the sausage perturbations can be unstable, while the kink perturbations are always stable. If $\omega_-^2 < 0$, then

Figure 5. Square of the frequency (in arbitrary units) as a function of κ and φ for the slab problem. The continuous curve corresponds to $\omega^2 = 0$ and represents the transition between stable and MRT unstable modes. The circle indicates the position in the diagram of the maximum growth rate. In this plot, $\alpha = 10°$, $\chi = 1$, $\zeta = 100$, $\sigma = 3.65 \times 10^4$. (A color version of this figure is available in the online journal.)

the two roots of Equation (23) considered as a quadratic equation with respect to ω^2 have different signs. This is only possible when the free term of the quadratic equation (23) is negative. In the dimensionless variables this condition is written as

$$\kappa^2 \sigma^2 \{2\chi^2 \cos^2 \varphi \cos^2(\varphi - \alpha) + [\cos^4(\varphi - \alpha) \\ + \chi^4 \cos^4 \varphi] \tanh 2\kappa\} < (\zeta - 1)^2 \tanh 2\kappa. \tag{43}$$

This inequality can be rewritten as

$$f(\kappa) \equiv \kappa(X + Y \tanh 2\kappa]) - Z \frac{\tanh 2\kappa}{\kappa} < 0, \tag{44}$$

where

$$X = 2\chi^2 \cos^2 \varphi \cos^2(\varphi - \alpha),$$
$$Y = \cos^4(\varphi - \alpha) + \chi^4 \cos^4 \varphi, \tag{45}$$
$$Z = \sigma^{-2}(\zeta - 1)^2.$$

Differentiating the function $f(\kappa)$ we obtain

$$f'(\kappa) = X + Y \tanh 2\kappa + \frac{2\kappa Y}{\cosh^2 2\kappa} + \frac{Z[\sinh(4\kappa) - 4\kappa]}{2\kappa^2 \cosh^2 2\kappa}. \tag{46}$$

It follows from a well-known inequality $\sinh x > x$ for $x > 0$ that the last term on the right-hand side of this equation is positive. Hence, $f'(\kappa) > 0$. We also have $f(\kappa) \to -2Z < 0$ as $\kappa \to 0$ and $f(\kappa) \to \infty$ as $\kappa \to \infty$. This implies that there is exactly one number $\kappa_c(\varphi)$ such that $f(\kappa_c) = 0$. The quantity $\kappa_c(\varphi)$ is defined by the equation obtained from Equation (43) by substituting the sign "<" by "=." The inequality (43) is satisfied when $\kappa < \kappa_c(\varphi)$, and it is not satisfied otherwise. All perturbations with $\kappa > \bar{\kappa}_c = \max \kappa_c(\varphi)$ are stable. In general, we failed to calculate $\max \kappa_c(\varphi)$ analytically, so it must be done numerically.

An example of the dependence of the square of the frequency on κ and φ is shown in Figure 5. The value of $\sigma = 3.65 \times 10^4$ used to plot this figure can be obtained if we take, for example, $V_{Ae} = 10^3$ km s^{-1} and $a = 100$ km. It is interesting to compare this figure with the results for the single interface shown in Figure 3. The equilibrium parameters are exactly the same in the two plots, but now for the slab problem we have an additional parameter, which is the half width of the slab, denoted by a. The curve representing the transition between the stable
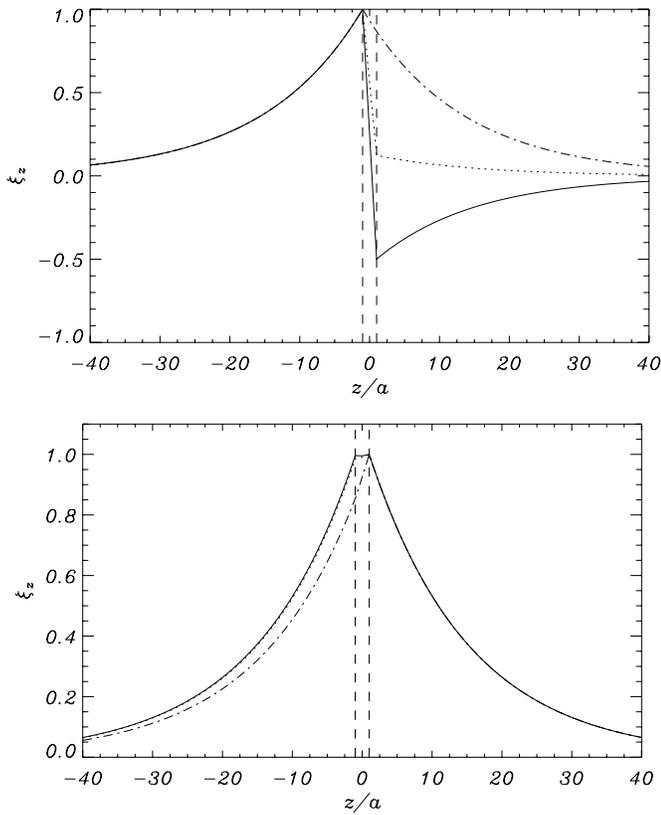
Figure 6. Eigenfunction for the ω_-^2 solution (top panel) and for the stable ω_+^2 solution (bottom panel) in the slab model. The continuous curve corresponds to an angle of propagation $\varphi = 80°$, the dotted curve to $\varphi = 90°$, and the dash-dotted to $\varphi = 100°$. A fixed dimensionless wave number $\kappa = 0.07$ has been selected to calculate the eigenfunctions. The rest of the parameters are the same as in Figure 5. The vertical dashed lines represent the slab boundaries. Note that some parts of the dotted and dash-dotted lines are superimposed on the solid lines and therefore not easy to distinguish. This happens on the left part of the top panel and on the right part of the bottom panel.

and the unstable regime of the ω_-^2 solution is slightly more complex for the slab problem and shows a double lobe structure around the maximum κ. The eigenfunctions for three different propagation angles are plotted in Figure 6 for a fixed κ and the same parameters as in Figure 5. In the top panel the ω_-^2 solution changes from stable (continuous curve) with a clear "sausage" character to unstable (dotted and dash-dotted lines). Note that eventually the eigenfunction of this mode is now localized at the lower interface. On the contrary, the solution corresponding to the ω_+^2, see bottom panel of Figure 6, has a clear "kink" profile, but it tends to be localized at the upper interface when φ is increased. Therefore the nature of the modes is closer to surface waves associated to the individual interfaces. Similar results were found in Terradas et al. (2012) in the absence of magnetic shear.

We concentrate now on the analysis of the growth time. In Figure 7 the dependence of τ_g associated to the most unstable mode is plotted as a function of α and V_{Ai} for a fixed value of χ, ζ, and a. The differences with respect to the interface results are that the curves of constant τ are essentially shifted down in the diagram (see Figure 4). This means that the slab configuration is more stable than the interface model. This diagram can be used as a diagnostic tool and clearly shows the dependence of the grow times in the space of parameters.

The stability analysis is greatly simplified in two limiting cases. In the first case the magnetic fields in the slab and external
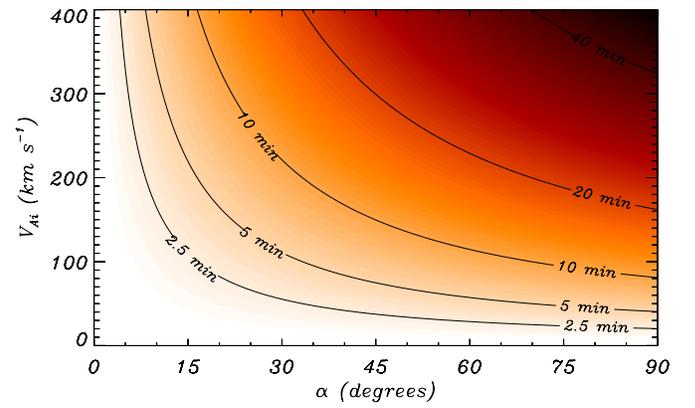
Figure 7. Growth time of the MRT instability for the slab problem as a function of the shear angle α and V_{Ai}. In this plot $\chi = 1$, $\zeta = 100$ and $a = 100$ km. (A color version of this figure is available in the online journal.)

regions are almost parallel, $\alpha \ll 1$, and $|\zeta - 1|/\sigma$ is of the order of unity. In this case it follows from the equation $f(\kappa) = 0$ that $\kappa_c(\varphi)$ takes moderate values when φ is not close to $\pi/2$, while it takes very large values when φ is close to $\pi/2$. Hence, to calculate $\bar{\kappa}_c$, it is enough to consider φ close to $\pi/2$. In accordance with this we put $\varphi = \pi/2 - \psi$ and assume that $|\psi| \ll 1$. In addition, since $\kappa_c \gg 1$, we can take $\tanh 2\kappa_c \approx 1$. Then we obtain from the equation $f(\kappa) = 0$ the approximate expression

$$\kappa_c(\varphi) \approx \frac{|\zeta - 1|}{\sigma[(\psi + \alpha)^2 + \chi^2\psi^2]}. \tag{47}$$

It immediately follows that

$$\bar{\kappa}_c = \kappa_c(\varphi_c) \approx \frac{|\zeta - 1|(1 + \chi^2)}{\sigma\chi^2\alpha^2}, \quad \varphi_c \approx \frac{\pi}{2} + \frac{\alpha}{1 + \chi^2}. \tag{48}$$

It is also not difficult to obtain the asymptotic expression for ω_-^2 valid for $\alpha \ll 1$ and $|\varphi - \pi/2| \ll 1$. It is given by

$$\omega_-^2 \approx \frac{g\{\sigma\kappa^2[\chi^2\psi^2 + (\psi + \alpha)^2] - \kappa|\zeta - 1|\}}{a(\zeta + 1)}. \tag{49}$$

When deriving this expression we have assumed that $\kappa \gg 1$ because $|\omega_-^2|$ is of the order of g/a when $\kappa \sim 1$, while $|\omega_-^2| \gg g/a$ when $\kappa \gg 1$. The quantity ω_-^2 takes its minimum value at $\varphi = \varphi_c$ and $\kappa = (1/2)\bar{\kappa}_c$, and the maximum growth rate is given by

$$\gamma_m \approx \frac{|\zeta - 1|}{2\chi\alpha}\sqrt{\frac{g(1 + \chi^2)}{a\sigma(\zeta + 1)}}. \tag{50}$$

In terms of the internal Alfvén speed the previous expression reduces to

$$\gamma_m \approx \frac{g|\zeta - 1|}{2\alpha V_{Ai}}\sqrt{\frac{\chi^2 + 1}{\zeta(\zeta + 1)}}. \tag{51}$$

This is exactly the same as Equation (36) which corresponds to the interface result in the limit of small α. This confirms that the slab problem in the limit of $\kappa \gg 1$ reduces to the interface problem because the penetration scale given by $1/\kappa$ is rather small and the role of the upper interface is negligible for the unstable mode (see also the plot of the eigenfunctions in Figure 6). Again we see that the situation here is similar to one that we have in the case of a single interface: $\gamma_m \to \infty$ as $\alpha \to 0$, so, in the case of parallel magnetic field ($\alpha = 0$), the growth rate
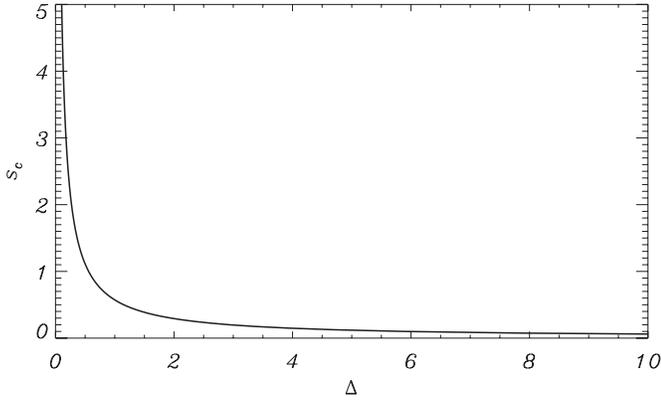
Figure 8. Dependence of s_c on Δ.

Figure 9. Dependence of Γ on Δ.

is unbounded and the initial value problem is ill-posed. On the other hand, the growth rate is bounded when the magnetic field is sheared ($\alpha \neq 0$), so the initial value problem is well-posed. As mentioned in the case of a single interface, the growth rate of the MRT instability in the model with parallel magnetic field ($\alpha = 0$) will be bounded and the problem will be well-posed if we take into account either dissipation or the finite thickness of the transitions between the three homogeneous regions.

Another limiting case where the analytic asymptotic analysis is possible is when $\zeta \gg 1$ and $\sigma \gtrsim \zeta^2$, while $\chi \simeq 1$ and $\alpha \simeq 1$. In this case it is not difficult to see from the equation $f(\kappa) = 0$ that $\kappa_c(\varphi) \ll 1$, so the equation $f(\kappa) = 0$ can be written in the approximate form as

$$\kappa^2[\cos^4(\varphi - \alpha) + \chi^4 \cos^4 \varphi] + \kappa \chi^2 \cos^2 \varphi \cos^2(\varphi - \alpha) = \zeta^2 \sigma^{-2}. \tag{52}$$

This equation is used in Appendix A to calculate φ_c. It is found that

$$\varphi_c = \varphi_{c1} \approx \frac{\pi}{2} + \frac{2\zeta \cot \alpha}{\sigma \chi^2},$$
$$\bar{\kappa}_c = \kappa_c(\varphi_{c1}) \approx \frac{\zeta}{\sigma \sin^2 \alpha} \tag{53}$$

when $\chi > 1$ and

$$\varphi_c = \varphi_{c2} \approx \frac{\pi}{2} + \alpha - \frac{2\zeta \cot \alpha}{\sigma},$$
$$\bar{\kappa}_c = \kappa_c(\varphi_{c2}) \approx \frac{\zeta}{\sigma \chi^2 \sin^2 \alpha} \tag{54}$$

when $\chi < 1$.

It is shown in Appendix B that the fastest growing mode propagates approximately perpendicular to the external magnetic field ($\varphi \approx \pi/2 + \alpha$). Its dimensionless wave number is equal to $\kappa_c = \zeta^{-1} s_c(\Delta)$, where

$$\Delta = \frac{\sigma \chi^2 \sin^2 \alpha}{\zeta^2}. \tag{55}$$

The dependence of s_c on Δ is shown in Figure 8. The instability increment is equal to

$$\gamma_m = (g/a\zeta)^{1/2} \Gamma(\Delta). \tag{56}$$

The dependence of Γ on Δ is plotted in Figure 9. All these results are obtained under the assumption that $\zeta \Delta > 1$, i.e., when $\chi^2 \sin^2 \alpha > \zeta/\sigma$.
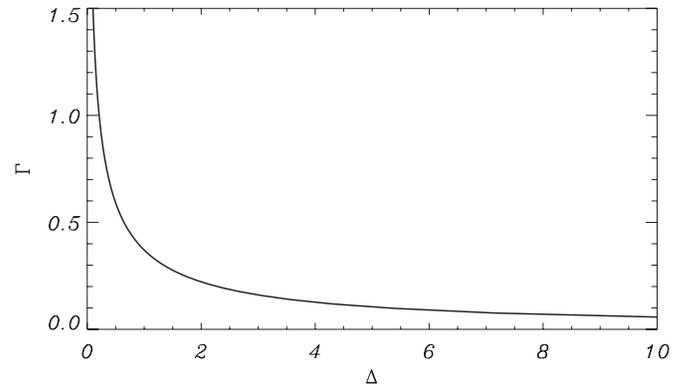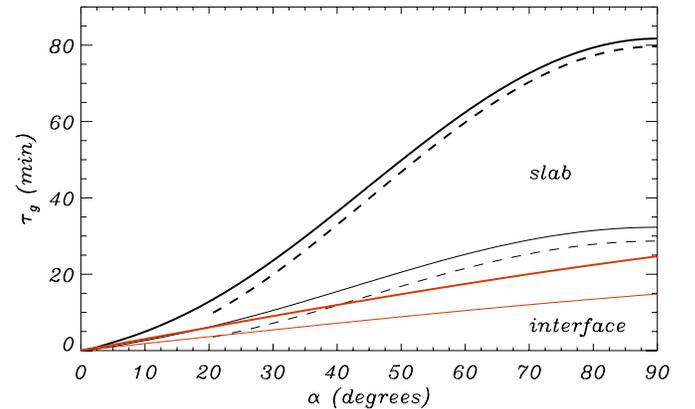

Figure 10. Growth time of the MRT instability for the slab problem (black color) and interface problem (red color) as a function of the shear angle α. The thin curves correspond to $\sigma = 1.45 \times 10^5$ ($V_{Ai} = 200 \, \text{km s}^{-1}$) while thick curves represent the case $\sigma = 5.2 \times 10^4$ ($V_{Ai} = 120 \, \text{km s}^{-1}$). Dashed lines correspond to the approximation in the slab problem for large angles given by Equation (56). In this plot $\chi = 1$ and $\zeta = 100$.

(A color version of this figure is available in the online journal.)

In Figure 10 the growth time of the instability calculated using the full solution (continuous curve) is plotted together with the approximation for finite angles (dashed curves) given by Equation (56). We do see a good match in the behavior of the two curves. The approximation slightly underestimates the growth time, and the differences increase when σ decreases. This is what we should expect if we recall that the approximation is based on the assumption $\sigma \gg 1$. We have already shown that, for small angles of the shear, the interface and the slab results are the same. Now this is also evident in Figure 10. This plot also shows that the differences in the growth time between the slab and the interface can be quite significant for $\alpha \simeq 1$.

5. APPLICATION TO OSCILLATING THREADS

The purpose of this section is to use the previous theoretical results to infer some information about the shear in real prominence threads. We consider the thread oscillation studied by Okamoto et al. (2007) using *Hinode*. These authors found threads oscillating vertically with periods around 4 min. Terradas et al. (2008) used these oscillations to do a seismological study of the thread. Although Okamoto et al. (2007) did not investigate the lifetime of the threads, from the movie of the event we estimate that threads do not last long. It is found that the typical lifetime is 10 min. The main idea here is to assume that the excitation of unstable modes is responsible for the short

lifetime of the structure. This MRT instability produces the disappearance of the structure. According to our results the fastest growing mode when there is magnetic shear has the following approximate growth time (see Equation (36))

$$\tau_g \approx \frac{\sqrt{2}}{g} V_{Ai} \alpha, \tag{57}$$

where we have assumed that $\zeta \gg 1$ and $\chi \approx 1$. This expression applies to the interface problem as well as to the slab problem (see Equation (51)), and it is valid in the limit of small α only. If the growth time is assumed to be around 10 min in order to use Equation (57) we must obtain a small angle, otherwise we get an inconsistent result. Terradas et al. (2008) found that the lower bound for the internal Alfvén speed is between 120 and 350 km s^{-1}. Nevertheless, some of the threads have high Alfvén velocities, up to 800 km s^{-1}, since they belong to an active region prominence. Let us assume that the velocity is around 500 km s^{-1} and calculate the corresponding shear angle. According to Equation (57) and using that $\tau_g = 10$ min and $V_{Ai} = 500$ km s^{-1} we obtain that $\alpha \approx 13°$. This angle is small and the application of Equation (57) is justified. This is in agreement with the behavior found in the more general expression given by Equation (35) which shows that α decreases when the internal Alfvén speed increases (see also Figure 4). In fact this expression shows that α is small for sufficiently large values of V_{Ai} but moderate for smaller values. For the present case of a velocity of $V_{Ai} = 500$ km s^{-1} the angle is small, and this is in accordance with the observations of prominence threads.

The observed oscillations of the thread are most probably kink oscillations. It is well known that the sausage waves in magnetic slabs and tubes have quite similar properties, while the properties of kink waves in slabs are quite different from those in tubes (e.g., Edwin & Roberts 1982, 1983). Since ω_+-mode is a kink mode, it is quite improbable that the observed disappearances of the thread are described by this mode. Note that, in the linear approximation, the kink oscillation of the thread does not interact with the unstable mode causing its disappearance, and thus it does not affect the instability growth time.

6. SUMMARY AND CONCLUSIONS

In the present paper we have extended the study by Terradas et al. (2012) to the models of an interface and a slab with magnetic shear, and have focused on the MRT instability. The fact that the magnetic field changes its direction introduces a bounded growth rate of the instability. This is different from the models without shear where the growth rate is unbounded. Because of this Terradas et al. (2012) concentrated on a particular wave number in the perpendicular direction equal to $1/a$, a being the half-thickness of the slab. Here we have focused on the maximum growth rate, representing the most unstable mode of the system, and have found analytical expressions in various limiting cases. For small angles of the shear the growth time is linearly proportional to the shear angle α. This applies to the single interface as well as to the slab problem. On the contrary, for large angles the growth time depends only weakly on α in the interface problem. In this limit, we have also been able to calculate an approximate expression for the growth time in the slab problem.

We have shown, using a simple example, how it is possible to estimate the shear angle in threads belonging to active region prominences from the combination of observations and the

theoretical results presented in this paper. Using this method we have found that the observations of oscillating threads of Okamoto et al. (2007) are compatible with small shear angles (around 13°). This indirect method of inferring some of the equilibrium properties of threads can be potentially used as a seismological tool.

Several simplifications have been done in the models considered in this work. Both the interface and slab configurations are unbounded in the perpendicular direction (y-direction) and we have assumed that there is dense material along the full length of the magnetic tube. However, in reality, threads only represent a small part of the full magnetic tube. Compressibility and partial ionization (see Díaz et al. 2012) have been also ignored. These basic assumptions in the models have enabled us to derive analytical expressions for the growth times. Nevertheless, the need for using improved models is obvious, and the study of the nonlinear evolution of the system is very relevant to assess the role of the MRT instability in the fast disappearance of threads.

APPENDIX A

CALCULATION OF φ_c AND $\bar{\kappa}_c$ FOR THE SLAB MODEL

In this appendix we calculate φ_c and $\bar{\kappa}_c$ for the slab model in the case where $\sigma \gg \zeta \gg 1$, while $\chi \simeq 1$ and $\alpha \simeq 1$. As it is shown in Section 4.2, in this case $\kappa_c(\varphi)$ is defined by the approximate equation (52). To calculate φ_c we differentiate equation (52) with respect to φ and then take $d\kappa/d\varphi = 0$. As a result we obtain

$$2\kappa[\chi^4 \cos^3 \varphi \sin \varphi + \cos^3(\varphi - \alpha) \sin(\varphi - \alpha)]$$
$$+ \chi^2 \cos \varphi \cos(\varphi - \alpha) \sin(2\varphi - \alpha) = 0. \tag{A1}$$

Eliminating κ from this equation and Equation (52) we obtain the equation for φ_c:

$$\sin \alpha \cos^2 \varphi \cos^2(\varphi - \alpha) \sin(2\varphi - \alpha)[\cos^4(\varphi - \alpha) - \chi^4 \cos^4 \varphi]$$
$$= \zeta^2 \sigma^{-2} \chi^{-4} \{\cos^2(\varphi - \alpha) \sin[2(\varphi - \alpha)] + \chi^4 \cos^2 \varphi \sin 2\varphi\}^2. \tag{A2}$$

Since $\zeta^2 \sigma^{-2} \ll 1$, to obtain the solution to this equation we use the regular perturbation method. In the first-order approximation we obtain that the left-hand side of Equation (A2) is zero. It is possible when one of the four multiplier that depend on φ is zero. We investigate these possibilities separately.

1. Let $\cos \varphi = 0$, i.e., $\varphi = \pi/2$. In the second-order approximation we look for the solution in the form $\varphi = \pi/2 - \psi$, where $|\psi| \ll 1$. Substituting this expression in Equation (A2) we easily calculate ψ and eventually obtain

$$\varphi_{1\pm} \approx \frac{\pi}{2} \pm \frac{2\zeta \cot \alpha}{\sigma \chi^2}. \tag{A3}$$

2. Let $\cos(\varphi - \alpha) = 0$, i.e., $\varphi = \pi/2 + \alpha$. In the second-order approximation we look for the solution in the form $\varphi = \pi/2 + \alpha - \psi$, where $|\psi| \ll 1$. Substituting this expression in Equation (A2) we, once again, easily calculate ψ and obtain

$$\varphi_{2\pm} \approx \frac{\pi}{2} + \alpha \pm \frac{2\zeta \cot \alpha}{\sigma}. \quad (A4)$$

3. Let $\sin(2\varphi - \alpha) = 0$, i.e., $\varphi = (1/2)\alpha$ or $\varphi = (\pi + \alpha)/2$. In the second-order approximation we look for the solution in the form $\varphi = (1/2)\alpha + \psi$, where $|\psi| \ll 1$. Substituting this expression in Equation (A2) we calculate ψ and obtain

$$\varphi_3 \approx \frac{\alpha}{2} + \frac{2\zeta^2(1 - \chi^4)}{\sigma^2 \chi^4} \tan \frac{\alpha}{2} \sec^3 \frac{\alpha}{2}. \quad (A5)$$

Similarly, looking for the solution in the form $\varphi = (\pi + \alpha)/2 + \psi$ with $|\psi| \ll 1$, we obtain

$$\varphi_4 \approx \frac{\pi}{2} + \frac{\alpha}{2} + \frac{2\zeta^2(\chi^4 - 1)}{\sigma^2 \chi^4} \cot \frac{\alpha}{2} \csc^3 \frac{\alpha}{2}. \quad (A6)$$

4. Let $\cos(\varphi - \alpha) = \pm\chi \cos\varphi$. It follows from this equation that

$$\varphi = \varphi_0 \equiv \arctan \frac{\pm\chi - \cos\alpha}{\sin\alpha}. \quad (A7)$$

In the second-order approximation we look for the solution in the form $\varphi = \varphi_0 + \psi$, where $|\psi| \ll 1$. Substituting this expression in Equation (A2), after some algebra, we obtain in the second-order approximation

$$\psi \sin\alpha \sin(2\varphi_0 - \alpha)[\pm\chi \sin\varphi_0 - \sin(\varphi_0 - \alpha)]$$
$$= \zeta^2\sigma^{-2}\chi^{-6}[\tan\varphi_0(\cos\alpha \pm \chi) - \sin\alpha]^2. \quad (A8)$$

Using Equation (A7) we derive the formulae

$$\sin(2\varphi_0 - \alpha) = \frac{\sin\alpha(\chi^2 - 1)}{1 \mp 2\chi \cos\alpha + \chi^2},$$
$$\pm\chi \sin\varphi_0 - \sin(\varphi_0 - \alpha) = \sqrt{1 \mp 2\chi \cos\alpha + \chi^2}. \quad (A9)$$

With the aid of Equations (A7) and (A9) we calculate ψ from Equation (A8). Finally we obtain

$$\varphi_{5\pm} \approx \arctan \frac{\pm\chi - \cos\alpha}{\sin\alpha}$$
$$+ \frac{\zeta^2(\chi^2 - 1)\sqrt{1 \mp 2\chi \cos\alpha + \chi^2}}{\sigma^2 \chi^6 \sin^4\alpha}. \quad (A10)$$

Hence, we have eight values of φ that are the solutions of Equation (52), and we have to choose one at that $\kappa_c(\varphi)$ takes its maximum value. To do this we have to calculate $\kappa_c(\varphi)$ at each of these eight values of φ using Equation (A1). The calculation is lengthy but straightforward, so we give only the final results:

$$\kappa_c(\varphi_{1\pm}) \approx \frac{\pm\zeta}{\sigma \sin^2\alpha}, \quad \kappa_c(\varphi_{2\pm}) \approx \frac{\mp\zeta}{\sigma \chi^2 \sin^2\alpha},$$

$$\kappa_c(\varphi_3) \approx \frac{2\zeta^2}{\sigma^2 \chi^2} \sec^5 \frac{\alpha}{2},$$

$$\kappa_c(\varphi_4) \approx \frac{2\zeta^2}{\sigma^2 \chi^2} \csc^5 \frac{\alpha}{2}, \quad \kappa_c(\varphi_{5\pm}) \approx -\frac{1}{2}. \quad (A11)$$

We disregard negative values of κ_c because we assumed from the very beginning that $\kappa > 0$. Since we have assumed that $\zeta/\sigma \ll 1$, it is straightforward to see that $\kappa_c(\varphi_{1+}) > \kappa_c(\varphi_3)$, $\kappa_c(\varphi_4)$ and $\kappa_c(\varphi_{2-}) > \kappa_c(\varphi_3)$, $\kappa_c(\varphi_4)$. Hence, eventually,

$$\bar{\kappa}_c \approx \kappa_c(\varphi_{1+}) \approx \frac{\zeta}{\sigma \sin^2\alpha}, \quad \chi > 1, \quad (A12)$$

and

$$\bar{\kappa}_c \approx \kappa_c(\varphi_{2-}) \approx \frac{\zeta}{\sigma \chi^2 \sin^2\alpha}, \quad \chi < 1. \quad (A13)$$

APPENDIX B

CALCULATION OF MAXIMUM INCREMENT

In this appendix we calculate the maximum growth rate of the Rayleigh–Taylor instability. In accordance with Equation (A1) the dimensionless wave number of an unstable mode is always small, $\kappa \lesssim \zeta/\sigma \ll 1$. This observation enables us to use the approximate Taylor expansions with respect to κ for functions $\tilde{F}$, $\tilde{G}$ and $\tilde{H}$:

$$\tilde{F} = \sigma\kappa^2\{[\chi^2 \cos^2\varphi + \zeta \cos^2(\varphi - \alpha)](1 + 2\kappa^2)$$
$$+ 2\kappa[\zeta\chi^2 \cos^2\varphi + \cos^2(\varphi - \alpha)]\}, \quad (B1)$$

$$\tilde{G} = \{\sigma^2\kappa^4[\chi^2 \cos^2\varphi - \zeta \cos^2(\varphi - \alpha)]^2 + 4\kappa^3\zeta^3(1 + \zeta\kappa)\}^{1/2}, \quad (B2)$$

$$\tilde{H} = 2\zeta(1 + \zeta\kappa). \quad (B3)$$

We introduce the dimensionless increment $\tilde{\gamma} = (g/a)^{1/2}|\omega_-|$. Then we obtain from Equation (39) the approximate equation

$$\tilde{\gamma}^2 = 2\kappa^3 \frac{\zeta^2 - \sigma^2\kappa\{\kappa[\chi^4 \cos^4\varphi + \cos^4(\varphi - \alpha)] + \chi^2 \cos^2\varphi \cos^2(\varphi - \alpha)\}}{\tilde{F} + \tilde{G}}. \quad (B4)$$

Now we investigate this expression in three various intervals of variation of the angle φ.

1. Let $\cos^2\varphi \simeq \cos^2(\varphi - \alpha) \simeq 1$, i.e., φ be not close to $\pi/2$ and to $\pi/2 + \alpha$. Then it follow from Equation (B4) that $\tilde{\gamma}^2 > 0$ only when $\kappa \lesssim \zeta^2/\sigma^2$. For these values of κ we have $\tilde{F} + \tilde{G} \gtrsim \zeta^5/\sigma^3$ and $\tilde{\gamma} \lesssim (\zeta/\sigma)^{3/2}$.

2. Let φ be close to $\pi/2$, so we take $\varphi = \pi/2 - \tilde{\varphi}$. Then we can use the approximate expression

$$\tilde{\gamma}^2 \approx 2\kappa^2 \frac{\zeta^2 - \sigma^2\kappa \sin^2\alpha(\kappa \sin^2\alpha + \chi^2\tilde{\varphi}^2)}{\sigma\zeta\kappa \sin^2\alpha + \zeta(\sigma^2\kappa^2 \sin^2\alpha + 4\zeta\kappa)^{1/2}}, \quad (B5)$$

It is obvious that, for any fixed κ, $\tilde{\gamma}^2$ takes its maximum value at $\tilde{\varphi} = 0$. When $\kappa \lesssim \zeta/\sigma^2$, we obtain $\tilde{\gamma}^2 \simeq \zeta^2/\sigma^3 \ll \zeta^2/\sigma^2$. On the other hand, we obtain $\tilde{\gamma}^2 \simeq \zeta^2/\sigma^2$ when $\kappa \simeq \zeta/\sigma$. Hence, when looking for the maximum value of $\tilde{\gamma}$, we can take $\tilde{\varphi} = 0$ and $\kappa \simeq \zeta/\sigma$. In that case $\sigma^2\kappa^2 \sin^2\alpha \gg 4\zeta\kappa$ and we can further reduce Equation (B5) to

$$\tilde{\gamma}^2 \approx \frac{\kappa(\zeta^2 - \sigma^2\kappa^2 \sin^4\alpha)}{\sigma\zeta \sin^2\alpha}. \quad (B6)$$

Then we easily find that the maximum value of $\tilde{\gamma}$ is given by

$$\tilde{\gamma}_m \approx \frac{\zeta}{\sigma \sin^2\alpha} \sqrt[4]{\frac{4}{27}}, \quad (B7)$$

9

and it is taken at

$$\kappa \approx \frac{\zeta}{\sqrt{3}\sigma \sin^2 \alpha}. \qquad (B8)$$

3. Let now φ be close to $\pi/2 + \alpha$, so we take $\varphi = \pi/2 + \alpha - \tilde{\varphi}$. Then we can use the approximate expression

$$\tilde{\gamma}^2 \approx 2\kappa^3 \frac{\zeta^2 - \sigma^2 \kappa^2 \chi^2 \sin^2 \alpha (\kappa \chi^2 \sin^2 \alpha + \tilde{\varphi}^2)}{\tilde{F} + \tilde{G}}, \qquad (B9)$$

where $\tilde{F}$ and $\tilde{G}$ are given by

$$\tilde{F} \approx \sigma \kappa^2 [\chi^2 \sin^2 \alpha (1 + 2\zeta\kappa) + \zeta \tilde{\varphi}^2], \qquad (B10)$$

$$\tilde{F} \approx [\sigma^2 \kappa^4 (\chi^2 \sin^2 \alpha - \zeta \tilde{\varphi}^2)^2 + 4\zeta^3 \kappa^3 (1 + \zeta\kappa)]^{1/2}. \quad (B11)$$

It is easy to show that $\tilde{F} + \tilde{G}$ is a monotonically increasing function of $\tilde{\varphi}^2$. Since the numerator in Equation (B9) is a monotonically decreasing function of $\tilde{\varphi}^2$, we conclude that, at a fixed κ, $\tilde{\gamma}$ takes its maximum value at $\tilde{\varphi} = 0$. Hence, we can take

$$\tilde{\gamma}^2 \approx \frac{2\kappa^2(\zeta^2 - \sigma^2 \kappa^2 \chi^2 \sin^4 \alpha)}{\sigma \kappa \chi^2 \sin^2 \alpha (1 + 2\zeta\kappa) + [\sigma^2 \kappa^2 \chi^4 \sin^4 \alpha + 4\kappa \zeta^3 (1 + \zeta\kappa)]^{1/2}} \qquad (B12)$$

when looking for the maximum value of $\tilde{\gamma}$. Introducing the new dimensionless variables

$$s = \zeta \kappa, \quad \Delta = \frac{\sigma \chi^2 \sin^2 \alpha}{\zeta^2}, \qquad (B13)$$

we obtain after some algebra

$$\tilde{\gamma}^2 = s \frac{[s^2 \Delta^2 + 4s(1+s)]^{1/2} - s\Delta(1+2s)}{2\zeta(1+s)}. \qquad (B14)$$

To calculate the maximum of function $\tilde{\gamma}^2(s)$ we have to find where its derivative is equal to zero. After some algebra the equation $d\tilde{\gamma}^2/ds = 0$ can be written as

$$2\Delta^4(2s^6 + 7s^5 + 8s^4 + 3s^3) + \Delta^2(16s^6 + 72s^5 + 119s^4 + 84s^3 + 19s^2 - 2s) - (4s^4 + 20s^3 + 37s^2 + 30s + 9) = 0. \quad (B15)$$

We consider this equation as a quadratic equation for Δ^2. The roots of this equation have different signs. Then, taking into account that $\Delta^2 > 0$, we obtain that s is defined by the equation

$$\Upsilon(s) = \Delta^2, \qquad (B16)$$

where $\Upsilon(s)$ is given by

$$\begin{aligned}
\Upsilon(s) = [s^2(2s^3 + 7s^2 + 8s + 3)]^{-1}[(256s^{10} + 2304s^9 \\
+ 9056s^8 + 20368s^7 + 28833s^6 + 26592s^5 \\
+ 15962s^4 + 6028s^3 + 1321s^2 + 140s + 4)^{1/2} \\
- (16s^5 + 72s^4 + 119s^3 + 84s^2 + 19s - 2)].
\end{aligned}$$
$$(B17)$$

It is straightforward to obtain that $\Upsilon(s) \to \infty$ as $s \to 0$ and $\Upsilon(s) \to 0$ as $s \to \infty$. We verified numerically that $\Upsilon(s)$ is a monotonically decreasing function. Hence, Equation (B16) has the single solution s_c for any value of Δ. The dependence of s_c on Δ is shown in Figure 8.

Since $\tilde{\gamma}^2(0) = 0$ and $\tilde{\gamma}^2(s) \to -\infty$ as $s \to \infty$ and it has only one extremum at $s = s_c$, this extremum is the maximum, i.e., $\tilde{\gamma}_m = \tilde{\gamma}(s_c)$. The dependence of $\Gamma = \zeta^{1/2}\tilde{\gamma}_n$ on Δ is shown in Figure 9.

Summarizing the analysis we see that the function $\tilde{\gamma}(\varphi, \kappa)$ has two local maxima. The first one is given by Equation (B7) and it is taken at $\varphi = \pi/2$ and κ given by Equation (B8). The second local maximum is given by Equation (B14) with $s = s_c$, and it is taken at $\varphi = \pi/2 + \alpha$ and $\kappa = \zeta^{-1}s_c$, where s_c is defined by Equation (B16). We temporarily denote the first local maximum as $\tilde{\gamma}_{m1}$ and the second as $\tilde{\gamma}_{m2}$. The absolute maximum of $\tilde{\gamma}(\varphi, \kappa)$ is equal to the larger of the two quantities $\tilde{\gamma}_{m1}$ and $\tilde{\gamma}_{m2}$.

Equation (B7) can be rewritten as

$$\tilde{\gamma}_{m1} \approx \frac{\chi^2}{\zeta \Delta} \sqrt[4]{\frac{4}{27}}. \qquad (B18)$$

Then it follows that

$$\frac{\tilde{\gamma}_{m1}}{\tilde{\gamma}_{m2}} \approx \frac{\chi^2}{\Delta \Gamma(\Delta)\sqrt{\zeta}} \sqrt[4]{\frac{4}{27}} \approx \frac{0.62\chi^2}{\Delta \Gamma(\Delta)\sqrt{\zeta}}. \qquad (B19)$$

It is not difficult to obtain the approximate expressions

$$s_c \approx \begin{cases} \dfrac{1}{2\Delta}, & \Delta \ll 1, \\[2ex] \dfrac{1}{\Delta\sqrt{6}}, & \Delta \gg 1, \end{cases} \qquad (B20)$$

Using this result we obtain

$$\Gamma \approx \begin{cases} \dfrac{1}{2\sqrt{\Delta}}, & \Delta \ll 1, \\[2ex] \dfrac{1}{\Delta}\sqrt{\dfrac{5}{6\sqrt{6}}}, & \Delta \gg 1, \end{cases} \qquad (B21)$$

We verified numerically that $\Delta\Gamma(\Delta)$ is a monotonically increasing function of Δ. Hence, it varies from $0.5\sqrt{\Delta}$ to $(5/6\sqrt{6})^{1/2}$ when Δ varies from very small value to ∞. Then it follows from Equation (B19) that $\tilde{\gamma}_{m1}/\tilde{\gamma}_{m2} \lesssim \chi^2(\zeta\Delta)^{-1/2}$. Hence, we conclude that $\tilde{\gamma}_{m1} \lesssim \tilde{\gamma}_{m2}$ for $\Delta > \chi^4/\zeta$. Since we assume that $\chi \simeq 1$, while the typical value of ζ is 100, we conclude that, for not very small values of Δ (say, $\Delta \gtrsim 0.1$), the absolute maximum of $\tilde{\gamma}$ is equal to $\tilde{\gamma}_{m2}$, i.e., $\tilde{\gamma}_m = \zeta^{-1/2}\Gamma(\Delta)$. It is taken at $\varphi \approx \pi/2 + \alpha$ and $\kappa \approx \zeta^{-1}s_c(\Delta)$.

REFERENCES

Bucciantini, N., Amato, E., Bandiera, R., Blondin, J. M., & Del Zanna, L. 2004, A&A, 423, 253
Chandrasekhar, S. 1961, Hydrodynamic and Hydromagnetic Stability (Oxford: Clarendon Press)
DeVore, C. R. 2012, in American Astronomical Society Meeting Abstracts (Washington, DC: American Astronomical Society), 220, 201.06
DeVore, C. R. 2013, in AAS/Solar Physics Division Meeting, AAS/Solar Physics Division Meeting (Washington, DC: American Astronomical Society), 44, 41
Díaz, A. J., Soler, R., & Ballester, J. L. 2012, ApJ, 754, 41
Edwin, P. M., & Roberts, B. 1982, SoPh, 76, 239
Edwin, P. M., & Roberts, B. 1983, SoPh, 88, 179
Goedbloed, J. P. 1971a, Phy, 53, 412
Goedbloed, J. P. 1971b, Phy, 53, 501
Goedbloed, J. P. 1971c, Phy, 53, 535
Goedbloed, J. P. H., & Poedts, S. 2004, Principles of Magnetohydrodynamics (Cambridge: Cambridge Univ. Press)

Hillier, A., Berger, T., Isobe, H., & Shibata, K. 2012a, ApJ, 746, 120
Hillier, A., Isobe, H., Shibata, K., & Berger, T. 2011, ApJL, 736, L1
Hillier, A., Isobe, H., Shibata, K., & Berger, T. 2012b, ApJ, 756, 110
Isobe, H., Miyagoshi, T., Shibata, K., & Yokoyama, T. 2005, Natur, 434, 478
Isobe, H., Miyagoshi, T., Shibata, K., & Yokoyama, T. 2006, PASJ, 58, 423
Jones, T. W., & De Young, D. S. 2005, ApJ, 624, 586
Jun, B.-I., & Norman, M. L. 1996, ApJ, 465, 800
Jun, B.-I., Norman, M. L., & Stone, J. M. 1995, ApJ, 453, 332
Okamoto, T. J., Tsuneta, S., Berger, T. E., et al. 2007, Sci, 318, 1577
O'Neill, S. M., De Young, D. S., & Jones, T. W. 2009, ApJ, 694, 1317
Parker, E. N. 1974, SoPh, 37, 127

Rayleigh, L. 1883, Proc. London Math. Soc., 14, 170
Roberts, B. 1981, SoPh, 69, 27
Robinson, K., Dursi, L. J., Ricker, P. M., et al. 2004, ApJ, 601, 621
Ryutova, M., Berger, T., Frank, Z., Tarbell, T., & Title, A. 2010, SoPh, 267, 75
Stone, J. M., & Gardiner, T. 2007, ApJ, 671, 1726
Taylor, G. I. 1950, RSPSA, 201, 192
Terradas, J., Arregui, I., Oliver, R., & Ballester, J. L. 2008, ApJL, 678, L153
Terradas, J., Oliver, R., & Ballester, J. L. 2012, A&A, 541, A102
Yang, B. L., Wang, L. F., Ye, W. H., & Xue, C. 2011, PhPl, 18, 072111
Zhang, P., Lau, Y. Y., Rittersdorf, I. M., et al. 2012, PhPl, 19, 022703